Chemical Engineering Journal 280 (2015) 41–48

Contents lists available at ScienceDirect

Chemical Engineering Journal

journal homepage: www.elsevier.com/locate/cej

Development of a chitin/graphene oxide hybrid composite for the removal of pollutant dyes: Adsorption and desorption study

Joaquín A. González [a], María E. Villanueva [a], Lidia L. Piehl [b], Guillermo J. Copello [a,*]

[a] Cátedra de Química Analítica Instrumental, Facultad de Farmacia y Bioquímica, Universidad de Buenos Aires (UBA), IQUIMEFA (UBA-CONICET), Junín 956, C1113AAD CABA, Argentina
[b] Cátedra de Física, Facultad de Farmacia y Bioquímica, Universidad de Buenos Aires (UBA), Junín 956, C1113AAD CABA, Argentina

HIGHLIGHTS

- The components' availability make this material a promising low-cost biosorbent.
- Oxidized groups in the nGO structure increase the reactivity of the hybrid.
- A hybrid composition endows it with adsorption versatility for acid and basic dyes.
- A high desorption degree could be achieve increasing the solution pH.
- Two powder components can be converged in a solid-like gel for adsorption processes.

ARTICLE INFO

Article history:
Received 20 March 2015
Received in revised form 28 May 2015
Accepted 29 May 2015
Available online 4 June 2015

Keywords:
Chitin
Graphene oxide nanosheets
Hybrid material
Pollutants dyes
Biosorbent

ABSTRACT

This work presents the synthesis of chitin (Chi) and chitin/graphene oxide (Chi:nGO) hybrid gels in mild conditions and their use as biosorbents in solid–liquid batch systems. The graphene oxide nanosheets, obtained from natural graphite through Hummers method, were characterized using FT-IR, ESR and pH_{pzc} determination as a qualitative approach of the degree of exfoliation and oxidation. Two kinds of widely used dyes were tested: Remazol Black (RB) as an acid dye model and Neutral Red (NR) as a basic dye model. Adsorption assays results were analyzed using two and three parameters isotherm models. The maximum adsorption capacity (q_m) for RB and NR were 9.3×10^{-2} mmol/g and 57×10^{-2} mmol/g being the first one reached by Chi and the second by the hybrid. Furthermore, the adsorption behavior over the time was evaluated through pseudo-first, pseudo-second, Elovich and Modified Freundlich models being the first one which described better all the cases except the adsorption of Remazol Black on chitin gel which follows an Elovich tendency. According to the pseudo-first order model, the uptake rates (k_1) were between 1.1×10^{-2} min^{-1} and 1.4×10^{-2} min^{-1}, but for the Chi:nGO-NR system it was 1.7×10^{-3} min^{-1}. The adsorption was observed to be dependent on both the solution pH and the Chi:nGO proportion. Finally, both dyes can be desorbed from both kinds of materials up to 60% of the sorbed amount by increasing the solution pH above 8. This would imply the capability of reutilization of the material with minor sorption capacity.

1. Introduction

Synthetics dyes have been widely used in textile, food, cosmetics, pharmaceutical industries and with microbiological purposes as well. With the development of technology and industry, more and more attention has been paid to dyes as water pollutants. The total dye production exceeds the 700,000 tons per year and about 2% of this production is discharged in effluent from manufacturing operations [1]. There are commonly about 10–15% of unused dyestuff entering the wastewater directly in the staining process but the loss of some reactive dyes in the dyeing process could reach 50% [2]. One of the major problems that water coloration entails is the reduction of sunlight transmission which affects photosynthesis and harms aquatic ecosystems [3]. In addition, many of the synthetic dyes are toxic and carcinogenic [4].

In the last years several wastewater treatment methods have been developed. Some examples of those techniques are coagulation, chemical oxidations and biological or enzymatic treatment.

* Corresponding author at: Química Analítica Instrumental, FFyB, UBA, Junín 956 – Piso 3, C1113AAD CABA, Argentina. Tel./fax: +54 11 49648254.
E-mail address: gcopello@ffyb.uba.ar (G.J. Copello).

http://dx.doi.org/10.1016/j.cej.2015.05.112
1385-8947/

However, most of them are not capable of achieving high quality treated water or carry high implementation costs [5]. Depending on the adsorbent source, adsorption technologies represent one of the most efficient and cheap alternatives towards the treatment of wastewater which may contain several kinds of pollutants, for instance dyes. Other advantages of these decontamination methods are the facile scaling-up, high efficiency sorption without releasing any co-product to the environment and the possibility of recovering the adsorbent once the treatment is finished in the case of liquid–solid adsorptions [6].

Several adsorbent materials have already shown the potential for dye adsorption [6–8]. Chitin and chitosan, by-products of alimentary industry, are considered low cost biosorbents and have been studied for the removal of dyes from aqueous media [9,10]. Chitin is the second most abundant biopolymer found in nature after cellulose and can be found in fungi, the exoskeleton of insects and the shells of crustaceans, including shrimp and crab, as well as other invertebrates, such as marine sponges [11,12]. Its structure consists predominantly of unbranched chains of β-(1 → 4)-2-acetoamido-2-deoxy-d-glucose.

Carbon, especially activated charcoal, has also been widely used in water purification processes due to its high porosity and specific surface. Currently, other carbon allotropes, such as graphene, carbon nanotubes and fullerene have acquired an important role in the development of new nanostructured materials with several applications in the water remediation field. Graphene, in particular, is a one-atom thick layer of graphite where the carbon atoms are distributed in a regular sp^2-bonded network [13]. One of the most important features of graphene to be taken into account for its potential use in wastewater treatment, and other adsorption processes, is its great specific surface (2630 m^2/g) and flat geometry [14]. These characteristics would allow the production of lightweight materials with high adsorption capacity using low amounts of graphene [15]. However, the poor solubility of graphene nanosheets, due to the lack of polar groups in its molecular structure, could represent a drawback when the adsorption of polar molecules is pursued. In order to avoid this disadvantage, a facile method for increasing the hydrophilicity and reactivity of graphene is the synthesis of graphene oxide (GO) nanosheets through oxidative exfoliation from cheap graphite [16]. Finally, several researchers have reported the use of GO as a filler for polysaccharide based materials, such as starch, alginate, agarose, cellulose and chitosan, mainly aiming for the reinforcement of mechanical properties [17–22].

In a previous work, we presented a novel hybrid material composed by chitin and graphene oxide nanosheets [23]. The importance of the addition of GO to the chitin matrix relies not only in the proven composite reinforcement but also in a potential improvement of the adsorption versatility due to the dissimilar chemical nature of both components. The obtaining of a solid-like gel from two powders make the hybrid a promising alternative for wastewater treatment in heterogeneous phase (batch or continuous systems) [9].

The aim of the present work was to evaluate the adsorption capabilities of chitin/graphene oxide hydrogels in liquid media against two different pollutant dyes: Remazol Black (RB) and Neutral Red (NR). The first was considered as a model of acidic dye due to the presence of sulfonic groups in its structure. On the other hand, the NR acts as a cationic or basic dye because of the highly protonable amines in its structure.

2. Experimental

2.1. Reagents and materials

Natural graphite powder (<125 mm particle size) was purchased from Bitter (UK). Chitin from crab shells (DA: 92%; Mr ≈400,000) was obtained from Fluka (USA). Calcium chloride dihydrate and methanol were purchased from Anedra (Argentina) and Sintorgan (Argentina), respectively. Dyes Remazol Black and Neutral Red were obtained from Sigma–Aldrich (USA) and Riedel-de Haën (Germany), respectively. All other reagents were of analytical grade.

2.2. Preparation of graphene oxide nanosheets

GO nanosheets were prepared through Hummers method as described elsewhere [24]. The resulting graphite oxide was exfoliated into GO monolayer nanosheets (nGO) by sonication at 35 kHz for 30 min after dispersion in citrate buffer (0.4 M; pH: 4.2). Then the suspension was centrifuged and the pellet was washed with water and then with methanol. The methanol was removed by heating in a stove at 60 °C and the graphene oxide powder was then stored at room temperature.

2.3. Preparation of chitin hydrogel and chitin/nGO hybrid materials

To prepare a transparent calcium solvent, 42.5 g of calcium chloride dihydrate was suspended in 50 mL of methanol and refluxed for 30 min at 82 °C to a state of near-dissolution. One gram of chitin powder was suspended in the calcium solvent and refluxed for 2 h at 90 °C with stirring [25].

Different mass ratios of chitin and nGO were mixed by thorough agitation in order to obtain four types of hybrid materials with different chitin to graphene oxide ratios (Chi:nGO): 3:1, 1.2:1, and 0.6:1. For example, 10 g of chitin suspension, containing 120 mg of pure chitin, was mixed with 40 mg of nGO in order to obtain a hybrid material with a Chi:nGO ratio of 3:1.

The chitin/nGO mixtures were poured between two glasses spaced by glass slides of known width and then submerged in methanol until they gelled. Finally, the gels were subjected to several water incubations in order to wash out all of the methanol and $CaCl_2$ residues. Blank chitin gels without nGO were obtained by a similar procedure and named Chi. All the gels were cut in a circular geometry with 5 mm diameter x 2 mm width for all the experiments.

2.4. Material characterization

In order to determine qualitatively the degree of exfoliation and oxidation of the nGO, it was analyzed by Fourier Transform Infrared Spectroscopy (FT-IR), Electron Spin Resonance (ESR) and the drift method. The graphite and nGO powders were placed in a capillary tube and ESR spectra were recorded at 20 °C in an X-band ESR Spectrometer Bruker EMX plus (Bruker Instruments, Inc., Berlin, Germany). The spectrometer settings included: sweep width 150.00 G; center field 3515 G; microwave power 10.0 mW and conversion time 5.12 ms. For g factor calculation, Diphenylpicrylhydrazyl (DPPH, Aldrich) (g = 2.0036) was used as an internal standard. FT-IR transmission spectra were acquired in the range 4000–400 cm^{-1} using a FTIR Spectrometer (Nicolet 360). All samples were previously dried for 24 h at 60 °C to avoid water related band interference. Scanning Electron Microscopy (SEM) images of freeze-dried and gold coated samples were taken using a FEI Quanta 200 microscope. The pH of the point of zero charge (pH_{pzc}) of nGO was determined by the drift method, where the pH point at which the curve of the final pH crosses the $pH_{initial} = pH_{final}$ line is the pH_{pzc} [26].

2.5. Adsorption experiments

Adsorption experiments were carried out by a batch method in a room with controlled temperature (25 °C) and constant stirring

(120 rpm). The effect of the medium pH, interaction times and adsorption isotherms were determined by sorbate decay in the solution supernatant. In the case of the isotherms analysis a weighted mass of hydrogel discs (corresponding to 5 mg dry weight) was added to an aqueous solution (5 mL) of RB or NR, ranging from 0.025 to 5 mM or 0.025 to 7 mM, respectively. Absorbance determinations were carried out at the characteristic absorption peak using an UV–Vis Spectrophotometer (Cecil CE 3021, Cambridge, England). The equilibrium adsorption capacity, q_e (mmol/g), for all experiments was determined by a mass balance on the dye:

$$q_e = \frac{(C_0 - C_e) \cdot V}{m} \quad (1)$$

where C_0 (mM) is the initial concentration, C_e (mM) is the equilibrium concentration in the liquid phase, V (L) is the volume of liquid phase, and m (mg) is the mass of the adsorbent.

All adsorption assays were carried out in plastic vessels. Blank experiments were conducted in order to verify the absence of sorbate precipitation and/or adsorption to the walls of the vessels.

2.6. Desorption study

Adsorbent discs were incubated with 5 mL of RB and NR solutions at saturation concentration, adjusted at optimum adsorption pH and stirred at 160 rpm at room temperature (25 °C) for 24 h. The amount of adsorbed dye was determined through the same method used in the adsorption experiments. Afterwards, all the discs were washed with ultrapure water several times until the residual water coloration was not significant. The adsorbents were then allowed to be in contact with 5 mL of buffer solution at different pH (7.0–10.0) for 24 h. The amount of desorbed dye was calculated from the concentration of desorbed dye in the liquid phase. The percentage of the dye desorbed from the adsorbents is calculated according to:

$$\text{Desorption} = \frac{\text{Mass desorbed}}{\text{Mass adsorbed}} \cdot 100 \quad (2)$$

2.7. Statistical analysis

All experiments and their corresponding measurements were conducted in triplicate under identical conditions and statistically analyzed by one-way ANOVA and by Bonferroni comparison post test if ANOVA $p < 0.05$.

3. Results and discussion

3.1. nGO and Chi:nGO characterization

The FTIR spectra of graphite and graphene oxide are shown in Supplementary data. The graphene oxide spectrum shows an increase in the bands corresponding to oxidized groups, which confirms the chemical exfoliation of graphite. In the spectrum of nGO, the slight band at 1240 cm^{-1} is attributed to the C–O–C bond stretching which demonstrates the formation of epoxy groups. The presence of carboxyl and carbonyl functional groups can also be detected at 1400 cm^{-1} and 1725 cm^{-1}, which corresponds to C–OH and C=O stretching, respectively [27].

The obtaining of nGO sheets by oxidation/exfoliation of graphite has also been evidenced by ESR. The Fig. 1 shows the ESR spectra of graphite and the resulting nGO. First, there is no shift in the position of the main peak located at $g = 2.0037$. Among the two spectra it is appreciable a 450 fold signal increase for the nGO peak. This result indicates an increment of moieties in the nGO structure which would be responsible for the increase in signal. Other researchers have proposed that these moieties would correspond to the oxidized groups such as –OH and –COOH produced during the oxidation of graphite [28]. In the case of bulk graphite the ESR line is Dysonian due to the skin effect, characteristic of conductive materials, whereas the nGO spectrum presents a single Lorentzian curve suggesting a loss of conductivity which represents another evidence of the introduction of defects in graphite structure due to oxidation [29]. In addition, an ESR spectrum of the GO produced by Hummers method was obtained before the final exfoliation stage. The non-exfoliated GO spectrum shows an overlapped sextet compatible with the signal of Mn^{2+}, as it could be observed in the inset of Fig. 1 [30]. After sonication in citrate buffer the sextet disappears and it is only appreciable the nGO peak without any shift in the magnetic field axis or changes in its shape or symmetry. This is mainly attributed to the citrate buffer washing step used to obtain the exfoliated GO nanosheets. During sonication, and subsequent centrifugation, the impurities from the graphite oxidation, including Mn^{2+}, are removed. This proves that the sonication in citrate buffer is useful not only for the nanosheets exfoliation but also for the removal of remnant impurities which could obstruct the adsorption sites of nGO. The Drift method was performed in order to obtain the pH_{pzc}, which is the pH value where the nGO has a net charge equal to zero (Supplementary data). Taking into account that the graphite pH_{pzc} is approximately 7.0 [31], the low pH_{pzc} obtained for nGO (below pH 2.0) would account for the appearance of acidic groups in the nGO sheets.

SEM images were used to observe the topography of the materials and how it is altered by the addition of nGO (Supplementary data). Chi has a smooth and homogeneous surface that is lost as the amount of nGO increases.

3.2. Effect of pH and Chi:nGO ratio on adsorption behavior

The influence of aqueous solution pH and Chi:nGO ratio on the adsorption of the two dyes was investigated in the pH range 4.0–8.0 (Fig. 2). For both dyes different adsorption behavior could be observed depending on the solution pH. RB is an acidic dye and its major adsorption on all the materials is evidenced in solutions with low pH (Fig. 2a). The *pKa* values of the RB are 3.8 and 6.9 attributed to the sulfone groups [32]; the pKa of the sodium sulfonate groups (–SO_3Na, i. e. sulfonic groups) present in the azodye are below pH 1.0. Thus, the RB is already negatively charged in the

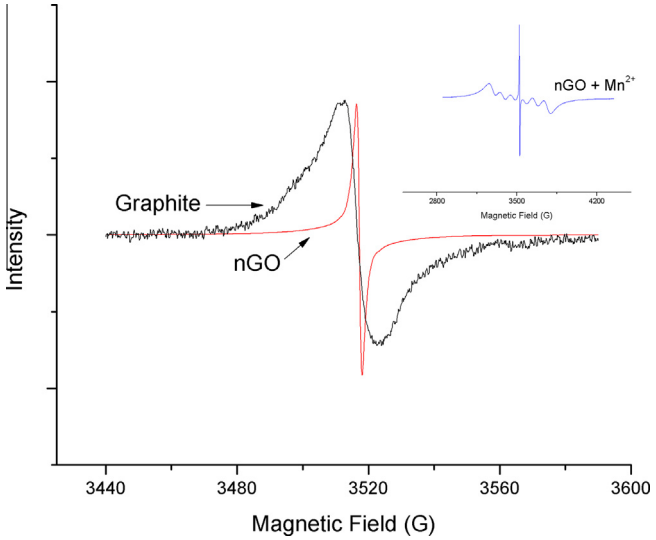

Fig. 1. ESR spectra of graphite and nGO.

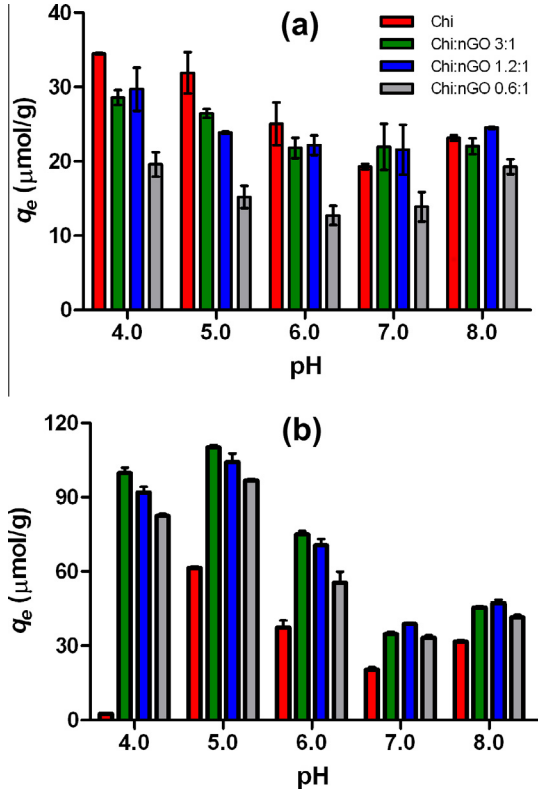

Fig. 2. Effect of pH in adsorption of RB (a) and NR (b) on different Chi:nGO proportion materials.

pH window tested. At pH 4.0 and 5.0 it could be considered that the charge density of the dye is almost the same. Regarding the Chi:nGO ratio, this could explain why the materials with low proportions of nGO have no important changes in their adsorption capacities. However, from pH 4.0 to 5.0 the sorption decrease among the high nGO proportion materials Chi:nGO 1.2:1 and 0.6:1 is appreciable. This occurs because the electrostatic repulsion between the dye molecules and the nGO (pH_{pzc} < 2.0) increases with the rise of the latter. At pH ⩾ 6.0 the adsorption capacity of all the materials, including Chi, reduces significantly probably due to a minor interaction of the RB with chitin matrix. In the case of Chi gels, since chitin has weakly chargeable functional groups in its molecular structure, it is proposed a non-ionic interaction between the polysaccharide and the RB that is less probable to occur at high pH values. Above pH 7.0 the negative charge of RB increases rising its solubility which explains why the affinity to the adsorbents is lower.

In the case of NR, there is a great difference between the adsorption capacities of Chi and the Chi:nGO hybrids, especially at pH 4.0 when the NR is highly positive charged (Fig. 2b). This explains why at pH 4.0 the Chi:nGO materials have an adsorption capacity much greater in comparison with Chi. At this pH, the NR is strongly attracted to the acid groups in nGO by electrostatic forces. Nevertheless, NR adsorption capacity is higher in those materials with low amounts of the carbon allotrope. This could be explained based on the dispersion of the nanosheets which tend to autoassociate at high concentrations leading to a less available interaction surface. On the other hand, a hydrogen bond interaction between NR and chitin is proposed, therefore when the dye is completely positively charged the electronic pairs of the nitrogens present in the molecule are unable to interact with chitin through hydrogen bonds. However, at pH 5.0 the adsorption on Chi increases significantly mainly due to the reduction of the positive density of the NR. Thus, its nitrogens become more available to interact with chitin. At high pH, the positive charge of the dye reduces followed by a drop of the hybrids' q_e. Taking into account the adsorption vs pH behavior the adsorption isotherms and kinetic studies were performed within the optimum pH.

Chi:nGO 3:1 was chosen as the most appropriate material for the isotherm, kinetic and desorption following experiments based on the high adsorption capacity and good mechanical properties. Moreover, the low nGO proportion would mean a lower nanosheets stacking providing a more homogeneous material with a higher specific surface.

3.3. FT-IR analysis of sorbed dyes

The pristine dyes spectra are presented in Supplementary data and the Chi, Chi-NR and Chi-RB spectra are represented in Fig. 3. In the three spectra the typical bands corresponding to chitin can be observed [33]. In the case of Chi-NR spectrum it can be seen an increment in the relative intensity of the 1080 cm^{-1} band (corresponding to the C–O–C stretching of the glycosidic bond) suggesting that this dye could interact with the glycosidic bond of the polysaccharide in a non-covalent way (Fig. 3a). This would agree with the formation of a hydrogen bond between Chi and NR proposed in the previous section. Regarding the Chi-RB spectrum, it does not have differences compared to the Chi spectrum despite the high adsorption capacity. This could be attributed to the masking of the major bands of RB (S═O stretching at 1140 cm^{-1} and ionic sulfate at 1250 cm^{-1}) with the strong glycosidic bond band of Chi around 1080 cm^{-1} [34]. The Fig. 3b shows the FT-IR spectra of Chi:nGO 3:1 and the hybrid with both dyes adsorbed. In the case of Chi:nGO-NR the only difference respect to the spectra of Chi:nGO is an increase in the adsorption of the NR bands at 1320 cm^{-1} and 1620 cm^{-1} due to the C–N bond and the primary amine, respectively [34]. Besides that, there is not any new appreciable signal or shift of any preexistent one suggesting that the interaction between NR and the adsorbent does not involve the formation of new covalent bonds or the appearance of a new functional group. Finally, there is no appreciable differences between the spectra of Chi:nGO and Chi:nGO-RB, probably due to the small amount of dye adsorbed to the material.

3.4. Adsorption isotherms

Adsorption isotherms were carried out at pH 4.0 and 5.0 for RB and NR, respectively. Those pH values were chosen based on the results of the adsorption vs pH experiment. All the absorbance measurements were done once the equilibrium was achieved and the results were expressed as q_e (mmol/g), i.e. millimole of sorbate per gram of adsorbent, against dye concentration at equilibrium (mM). In order to obtain a better description of the adsorption process, all the results were analyzed through the non-linear form of four two-parameters isotherm models (Langmuir, Freundlich, Dubinin–Radushkevich and Temkin) and two three-parameters models (Redlich–Peterson and Sips) [35,36]. Furthermore, the goodness-of-fit was evaluated by the root mean square error (RMSE) [37].

In Supplementary data all the assessed models with their non-linear equations and a Table that summarizes all the parameters and RMSE of each one are shown. The Fig. 4 exhibits the adsorption curves of both dyes on the different materials whereas Table 1 shows the results of all the adsorption systems presenting the model that adjusts better and the Langmuir parameters with the aim of assessing and comparing the maximum capacity (q_m) and affinity constant (K_a) to each sorbate. In the case of RB, the gel Chi showed a better adjustment to the Redlich-Peterson model which is considered as an extension of the Langmuir isotherm [38];

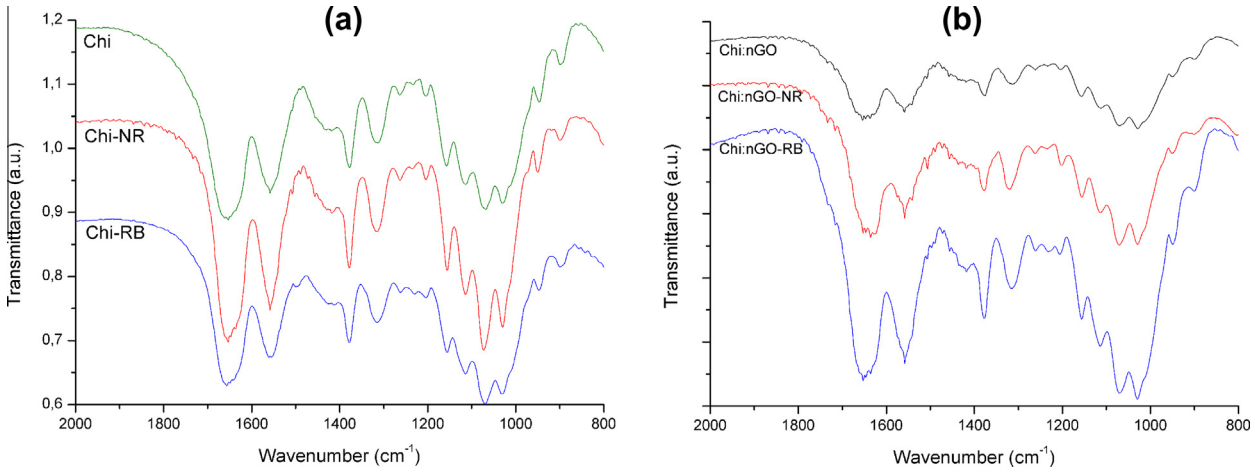

Fig. 3. FT-IR spectra of Chi (a) and Chi:nGO 3:1 (b) loaded with RB and NR.

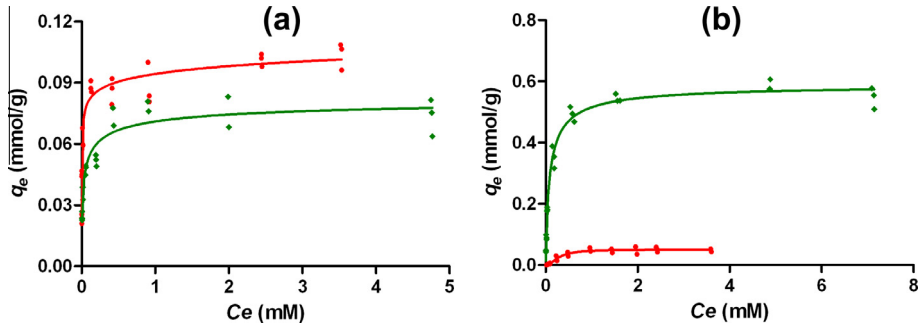

Fig. 4. Adsorption isotherms of RB (a) and NR (b) at pH 4.0 and 5.0 respectively. Only the best fitted models are represented. Chi (●) Chi:nGO 3:1 (♦).

Table 1
Best fitted isotherms models and Langmuir parameters.

Material – Dye	Best model					Langmuir		
	Model	Parameters			RSME	q_m (mmol/g)	K_a (L/mmol)	RSME
Chi – RB	R–P	K_{RP} (L/mmol)	α_{RP} ((L/mmol)^{nRP})	n_{RP}		$(9.3 \pm 0.26) \times 10^{-2}$	301 ± 56	9.91×10^{-3}
		44 ± 11	469 ± 120	0.94 ± 0.02	8.02×10^{-3}			
Chi:nGO 3:1 – RB	Sips	q_{mS} (mmol/g)	K_S (L/mmol)	n_S		$(7.1 \pm 0.30) \times 10^{-2}$	63 ± 16	9.53×10^{-3}
		$(8.5 \pm 0.9) \times 10^{-2}$	32 ± 18	0.5 ± 0.1	6.99×10^{-3}			
Chi – NR	Sips	q_{mS} (mmol/g)	K_S (L/mmol)	n_S		$(5.9 \pm 0.5) \times 10^{-2}$	2.4 ± 0.7	7.75×10^{-3}
		$(5.0 \pm 0.3) \times 10^{-2}$	3.5 ± 0.6	2.0 ± 0.6	6.90×10^{-3}			
Chi:nGO 3:1 – NR	Sips	q_{mS} (mmol/g)	K_S (L/mmol)	n_S		$(57 \pm 1) \times 10^{-2}$	12 ± 2	3.48×10^{-2}
		$(59 \pm 2) \times 10^{-2}$	11 ± 2	0.80 ± 0.08	3.19×10^{-2}			

since its heterogeneity parameter is close to 1 ($n_{RP} = 0.94 \pm 0.02$) it is suggested that the adsorption tends to a Langmuir behavior, i.e. a relative homogeneous adsorption in a monolayer distribution. In the case of the system Chi:nGO 3:1-RB, it adjusted better to the Sips model which combines characteristics of Langmuir and Freundlich depending on the concentration of sorbate. At low concentrations of sorbate it effectively reduces to a Freundlich isotherm and thus does not obey Henry's law. At high sorbate concentrations, it predicts a monolayer sorption capacity characteristic of the Langmuir isotherm [39]. Like R–P model, Sips has a heterogeneity parameter represented by n_s which is far from 1 ($n_s = 0.5 \pm 0.1$) suggesting a heterogeneous sorption. In addition, the Chi-RB Langmuir parameters exhibit a slightly higher adsorption capacity and a K_a five times higher in comparison to the hybrid Chi:nGO. These two kinds of adsorption behavior of the same dye on two different materials could be explained in terms of the composition of each gel. In the case of Chi, it would have more homogeneous adsorption sites and more affinity to RB compared to Chi:nGO because the hybrid has GO nanosheets dispersed among the chitin matrix and are negatively charged at this sorption pH. Therefore, the nGO contributes not only to the heterogeneity of the material but also to the electrostatic repulsion of the RB.

On the other hand, the NR adsorption adjusted better to Sips in both gels with a major degree of homogeneity in the case of the hybrid. It could be seen that the Chi:nGO 3:1 q_m and K_a widely exceed Chi ones. This is due to the presence of the nanosheets that are negatively charged at pH 5.0. The nGO functional groups (for instance carboxyl residues), distributed across the nanosheet surface, provide an electrostatic attraction to NR which is positively charged at low pH. Moreover, the addition of nGO to the matrix

represents an increment of potential adsorbent surface of the material explaining the higher capacity.

Finally, Table 2 presents the maximum adsorption capacities of RB and NR of several adsorbents reported in literature [7,17,40–43]. Those materials were selected based on their composition. As it can be observed, most of them contain one of the components that are presented in this work or at least a derivative one. The comparison assessment demonstrates that either Chi and Chi:nGO 3:1 materials present similar or higher adsorption performances toward RB and NR considering their low-cost and ease of synthesis. In the cases where the q_m is higher than for the Chi:nGO hybrid, the sorbents contain more processed components, such as those that use chitosan.

3.5. Adsorption kinetics

Adsorption kinetics results are shown in Fig. 5. These plots show the adsorption capacities over time. In order to analyze the dyes' uptake rates a simple kinetic analysis using the pseudo-first order, pseudo-second order, Elovich and modified Freundlich equations were performed in their non-linear forms [44–47]. Table 3 summarizes the parameters of every model. The mathematical kinetic equations and their description are presented in Supplementary data. As in the isotherm experiments, the adequacy of the nonlinear models adjustment was determined by the RMSE selection criteria.

The model that describes better the adsorption of RB on Chi gel is Elovich model, followed by pseudo-second order, modified Freundlich and pseudo-first order, in that order. The Elovich model, usually applied to the description of chemisorption processes, assumes that the reactive sites of the biosorbent are heterogeneous and thus present different activation energies based on a second-order reaction mechanism for a heterogeneous process reaction [47].

In the RB kinetic sorption using Chi:nGO 3:1 as adsorbent and NR using both materials, the model that describes better all the mentioned cases is the pseudo-first order model. These results would prove that in those cases the sorption process is independent of the free sites of interaction which are considered unlimited or constant. Furthermore, the kinetic of sorption would be lead by only one predominant step [46].

Table 2
Comparative table showing the maximum adsorption capacities (q_m) of different materials after adsorption of RB and NR.

Dye/Adsorbent	q_m (mg/g)	Ref.
Remazol Black		
Graphite oxide/chitosan composite	277	[7]
Chi	92	This work
Carbon from sugar beet pulp	80	[17]
Chi:nGO 3:1	70	This work
Activated carbon	59	[39]
Neutral Red		
Chitosan/TEOS hydrogel	254	[40]
Chi:nGO 3:1	165	This work
GO–Fe_3O_4 hybrid	141	[41]
Rectorite/F_3O_4 nanocomposite	46	[42]
Chi	17	This work

3.6. Desorption analysis

The results exhibited in Fig. 6 show the effect of solution pH on the dyes desorption. RB desorption increases as pH is higher in both cases. First, the RB desorption from Chi increases until pH 9.0 (Fig. 6a). As it was described before, an increment in the solution pH favors the solubility of RB reducing the interaction with the chitin matrix. In the case of Chi:nGO 3:1, the desorption behavior vs pH may be explained according to the acid-base nature of RB; the more alkaline is the medium, the greater is the negative charge density of the dye hence the electrostatic repulsion with nGO is higher. Nevertheless, the desorption percentage at pH 10.0 fell in both cases. This could be attributed to the dyeing mechanism of the azodye RB. At pH above 9.0 the 2-sulfatoethylsulfone moiety present in the RB molecular structure is hydrolyzed into a vinyl sulfone group (even at room temperature) which is able to react against –OH residues through a nucleophilic addition reaction [48]. Therefore, a lower desorption at pH 10.0 is expected considering the great amount of hydroxyl groups present in the chitin chains and the nGO functional groups which could generate a new covalent bond with RB.

At pH 7.0 the desorption percentage of NR from Chi could be considered low in comparison to the great amount of dye desorbed from pH 8.0 (Fig. 6b). Between pH 7.0 and 8.0, NR suffers a deprotonation which is detectable as a change in the solution color (from red to yellow), that is the main characteristic of this dye used as pH indicator. After the deprotonation, the molecular structure is stabilized by resonance and one of the predominant structures is a quinone imine which has less available nitrogens to establish hydrogen bonds with chitin. The dye desorption from Chi:nGO increases as the solution turns more and more alkaline reaching a maximum desorption value of 56%. This behavior sustains the results obtained in the previous adsorption at different pH experiment and it could be concluded that the principal interaction force that lead the adsorption onto Chi:nGO hybrid is the ionic interaction between NR and nGO. Probably other weaker interactions, such as van der Waals attraction and π–π interactions, are predominant at higher pH levels where NR is found as a neutral molecule, and keep some dye adsorbed to the material. From Fig. 6 it could also be observed that the dye desorption from the Chi-nGO material is near to 60% for both cases. This would mean that the hybrid could be reused for further adsorption cycles but with less capacity than in the first incubation. That degree of RB desorption is comparable or slightly lower than similar previously reported materials, such as cross-linked chitosan [49]. However, Chi:nGO 3:1 shows a higher desorption of NR compared to a chemically similar

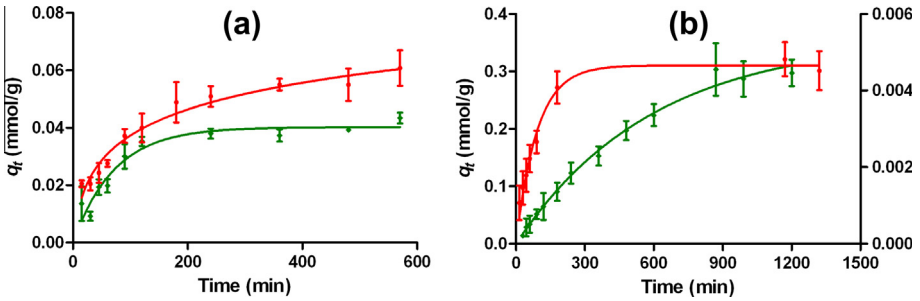

Fig. 5. Adsorption kinetics of RB (a) and NR (b) at pH 4.0 and 5.0 respectively. Only the best fitted models are represented. Chi (●) Chi:nGO 3:1 (♦). q_t (±SD, $n = 3$).

Table 3
Kinetic model parameters.

Model	Parameter	Material – Dye			
		Chi – RB	Chi:nGO 3:1 – RB	Chi – NR	Chi:nGO 3:1 – NR
Pseudo-first order	q_e (mmol/g)	$(5.6 \pm 0.2) \times 10^{-2}$	$(4.0 \pm 0.1) \times 10^{-2}$	$(4.7 \pm 0.2) \times 10^{-3}$	0.35 ± 0.02
	k_1 (min^{-1})	$(1.2 \pm 0.1) \times 10^{-2}$	$(1.4 \pm 0.1) \times 10^{-2}$	$(1.1 \pm 0.1) \times 10^{-2}$	$(1.7 \pm 0.2) \times 10^{-3}$
	RSME	5.17×10^{-3}	3.98×10^{-3}	4.09×10^{-4}	2.12×10^{-2}
Pseudo-second order	q_e (mmol/g)	$(6.5 \pm 0.2) \times 10^{-2}$	$(4.7 \pm 0.2) \times 10^{-2}$	$(5.0 \pm 0.2) \times 10^{-3}$	0.53 ± 0.05
	k_2 (g/(mmol.min))	0.22 ± 0.04	0.34 ± 0.06	2.8 ± 0.5	$(2.3 \pm 0.6) \times 10^{-3}$
	RSME	4.53×10^{-3}	4.15×10^{-3}	4.28×10^{-4}	2.17×10^{-2}
Elovich	α (mmol/(g.min))	$(1.9 \pm 0.4)x10^{-3}$	$(1.4 \pm 0.4)x10^{-3}$	$(1.7 \pm 0.5)x10^{-4}$	$(1.9 \pm 0.4)x10^{-3}$
	β (g/mmol)	73 ± 6	100 ± 10	1131 ± 113	5.3 ± 0.7
	RSME	4.35×10^{-3}	4.60×10^{-3}	5.32×10^{-4}	2.23×10^{-2}
Modified Freundlich	k_f (L/(mmol.min))	$(3.4 \pm 0.4) \times 10^{-2}$	$(2.4 \pm 0.4) \times 10^{-2}$	$(3.1 \pm 0.5) \times 10^{-3}$	$(1.4 \pm 0.3) \times 10^{-2}$
	m	3.2 ± 0.2	3.2 ± 0.3	3.9 ± 0.4	1.6 ± 0.9
	RSME	4.71×10^{-3}	5.17×10^{-3}	6.31×10^{-4}	2.54×10^{-2}

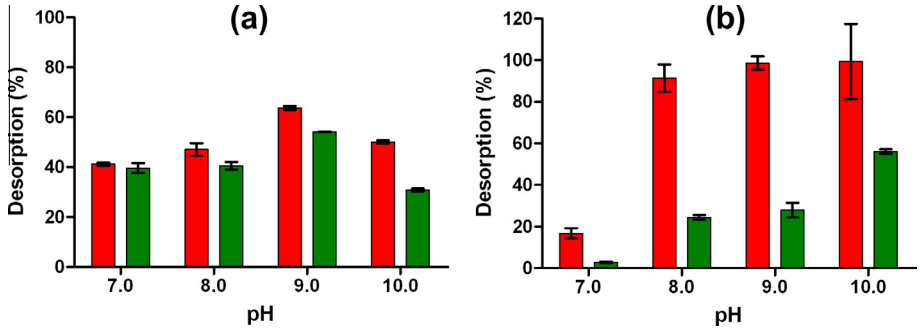

Fig. 6. Desorption of RB (a) and NR (b) at different pH. Chi (red column), Chi:nGO 3:1 (green column). Desorption (%) (±SD, $n = 3$). (For interpretation of the references to color in this figure legend, the reader is referred to the web version of this article.)

material such as magnetic multiwall carbon nanotubes (MWCNT). nanocomposite [50].

4. Conclusion

Both types of gels obtained in this work were able to adsorb the acidic and basic dyes. It was demonstrated that the adsorption capacities of chitin and hybrid gels against both pollutants is pH and Chi:nGO proportion dependent. NR and RB showed an optimum adsorption pH of 5.0 and 4.0 respectively. Chi:nGO 3:1 was chosen as the most appropriate material for the isotherm, kinetic and desorption experiments based on the high adsorption capacity and good mechanical properties. Despite of the lower adsorption capacity for the acidic dye of the hybrid in comparison to the Chi gel, the nGO addition would be necessary to endow the material with optimal mechanical properties. Hence, the amount of nGO in the hybrid would imply a compromise between mechanical resistance and adsorption behavior. The model which showed to have a good fitting for all systems was the Sips model except to Chi-RB which followed the Redlich–Peterson model. The uptake rate of RB and NR showed a similar kinetic behavior regardless of the adsorbent material. However, the Chi-RB system fitted better to the Elovich equation meanwhile the other systems adjusted better to the pseudo-first model. For all the loaded materials, the optimal desorption pH values of RB and NR were 9.0 and 10.0 respectively; this would mean an advantage if reuse of the adsorbents is pursued.

Acknowledgments

J.A.G. is grateful for his doctoral fellowship granted by UBA. M.E.V. is grateful for her doctoral fellowship granted by CONICET. This work was supported with grants from UBA (UBACYT 20020130100780) and CONICET (PIP 11220120100657CO). The authors would like to thank I. Pickering for language corrections.

Appendix A. Supplementary data

Supplementary data associated with this article can be found, in the online version, at http://dx.doi.org/10.1016/j.cej.2015.05.112.

References

[1] T. Robinson, G. McMullan, R. Marchant, P. Nigam, Remediation of dyes in textile effluent: a critical review on current treatment technologies with a proposed alternative, Bioresour. Technol. 77 (2001) 247–255.
[2] C. O'Neill, F.R. Hawkes, D.L. Hawkes, N.D. Lourenço, H.M. Pinheiro, W. Delée, Colour in textile effluents – sources, measurement, discharge consents and simulation: a review, J. Chem. Technol. Biotechnol. 74 (1999) 1009–1018.
[3] M.T. Sulak, E. Demirbas, M. Kobya, Removal of Astrazon Yellow 7GL from aqueous solutions by adsorption onto wheat bran, Bioresour. Technol. 98 (2007) 2590–2598.
[4] H. Li, J. Wan, Y. Ma, Y. Wang, M. Huang, Influence of particle size of zero-valent iron and dissolved silica on the reactivity of activated persulfate for degradation of acid orange 7, Chem. Eng. J. 237 (2014) 487–496.
[5] Y. Anjaneyulu, N. Sreedhara Chary, D. Samuel Suman Raj, Decolourization of industrial effluents – Available methods and emerging technologies – A review, Rev. Environ. Sci. Biotechnol. 4 (2005) 245–273.
[6] M.M. Nassar, M.S. El-Geundi, Comparative cost of colour removal from textile effluents using natural adsorbents, J. Chem. Technol. Biotechnol. 50 (1991) 257–264.
[7] G.J. Copello, A.M. Mebert, M. Raineri, M.P. Pesenti, L.E. Diaz, Removal of dyes from water using chitosan hydrogel/SiO_2 and chitin hydrogel/SiO_2 hybrid materials obtained by the sol–gel method, J. Hazard. Mater. 186 (2011) 932–939.
[8] G. Crini, Non-conventional low-cost adsorbents for dye removal: a review, Bioresour. Technol. 97 (2006) 1061–1085.
[9] G.Z. Kyzas, M. Kostoglou, A.A. Vassiliou, N.K. Lazaridis, Treatment of real effluents from dyeing reactor: experimental and modeling approach by adsorption onto chitosan, Chem. Eng. J. 168 (2011) 577–585.
[10] R. Dolphen, N. Sakkayawong, P. Thiravetyan, W. Nakbanpote, Adsorption of Reactive Red 141 from wastewater onto modified chitin, J. Hazard. Mater. 145 (2007) 250–255.

[11] R.A.A. Muzzarelli, Chitin and its derivatives: new trends of applied research, Carbohydr. Polym. 3 (1983) 53–75.
[12] H. Ehrlich, M. Maldonado, K. Spindler, C. Eckert, T. Hanke, R. Born, et al., First evidence of chitin as a component of the skeletal fibers of marine sponges. Part I. Verongidae (demospongia: Porifera), J. Exp. Zoolog. B Mol. Dev. Evol. 308B (2007) 347–356.
[13] K.S. Novoselov, A.K. Geim, S.V. Morozov, D. Jiang, Y. Zhang, S.V. Dubonos, et al., Electric field effect in atomically thin carbon films, Science 306 (2004) 666–669.
[14] F. Bonaccorso, L. Colombo, G. Yu, M. Stoller, V. Tozzini, A.C. Ferrari, et al., Graphene, related two-dimensional crystals, and hybrid systems for energy conversion and storage, Science 347 (2015).
[15] T.S. Sreeprasad, S.M. Maliyekkal, K.P. Lisha, T. Pradeep, Reduced graphene oxide–metal/metal oxide composites: facile synthesis and application in water purification, J. Hazard. Mater. 186 (2011) 921–931.
[16] X. Yang, C. Chen, J. Li, G. Zhao, X. Ren, X. Wang, Graphene oxide-iron oxide and reduced graphene oxide-iron oxide hybrid materials for the removal of organic and inorganic pollutants, RSC Adv. 2 (2012) 8821–8826.
[17] N.A. Travlou, G.Z. Kyzas, N.K. Lazaridis, E.A. Deliyanni, Graphite oxide/chitosan composite for reactive dye removal, Chem. Eng. J. 217 (2013) 256–265.
[18] S. Debnath, A. Maity, K. Pillay, Magnetic chitosan–GO nanocomposite: synthesis, characterization and batch adsorber design for Cr (VI) removal, J. Environ. Chem. Eng. 2 (2014) 963–973.
[19] N.D. Luong, N. Pahimanolis, U. Hippi, J.T. Korhonen, J. Ruokolainen, L.-S. Johansson, et al., Graphene/cellulose nanocomposite paper with high electrical and mechanical performances, J. Mater. Chem. 21 (2011) 13991–13998.
[20] T. Ma, P.R. Chang, P. Zheng, X. Ma, The composites based on plasticized starch and graphene oxide/reduced graphene oxide, Carbohydr. Polym. 94 (2013) 63–70.
[21] H.-J. Koo, S.-K. Kim, P.V. Braun, Facile fabrication of graphene composite microwires via drying-induced size reduction of hydrogel filaments, RSC Adv. 4 (2014) 20927–20931.
[22] H.X. Liu, Y.Q. Tan, Q.X. Zhang, X. Qin, R.R. Zheng, K.Y. Sui, et al., Rheological behaviors of carbonaceous materials suspended in sodium alginate solutions, Adv. Mater. Res., Trans Tech Publ, 2014, pp. 232–237.
[23] J.A. Gonzalez, M.F. Mazzobre, M.E. Villanueva, L.E. Diaz, G.J. Copello, Chitin hybrid materials reinforced with graphene oxide nanosheets: chemical and mechanical characterisation, RSC Adv. 4 (2014) 16480–16488.
[24] W.S. Hummers, R.E. Offeman, Preparation of graphitic oxide, J. Am. Chem. Soc. 80 (1958) 1339.
[25] H. Tamura, H. Nagahama, S. Tokura, Preparation of Chitin hydrogel under mild conditions, Cellulose 13 (2006) 357–364.
[26] M.V. Lopez-Ramon, F. Stoeckli, C. Moreno-Castilla, F. Carrasco-Marin, On the characterization of acidic and basic surface sites on carbons by various techniques, Carbon 37 (1999) 1215–1221.
[27] R. Li, C. Liu, J. Ma, Studies on the properties of graphene oxide-reinforced starch biocomposites, Carbohydr. Polym. 84 (2011) 631–637.
[28] C.V. Pham, M. Krueger, M. Eck, S. Weber, E. Erdem, Comparative electron paramagnetic resonance investigation of reduced graphene oxide and carbon nanotubes with different chemical functionalities for quantum dot attachment, Appl. Phys. Lett. 104 (2014) 132102.
[29] R.L. Collins, M.D. Bell, G. Kraus, Unpaired electrons in carbon blacks, J. Appl. Phys. 30 (1959) 56–62.
[30] A.M. Panich, A.I. Shames, A.E. Aleksenskii, A. Dideikin, Magnetic resonance evidence of manganese–graphene complexes in reduced graphene oxide, Solid State Commun. 152 (2012) 466–468.
[31] M. Karthikeyan, K.P. Elango, Removal of fluoride from aqueous solution using graphite: a kinetic and thermo-dynamic study, Indian J. Chem. Technol. 15 (2008) 525.
[32] D. Lucio, D. Laurent, G. Roger, Adsorption of remazol black b dye on activated carbon felt, Carbon Sci. Technol. 12 (2008) 12–15.
[33] Y. Saito, J.-L. Putaux, T. Okano, F. Gaill, H. Chanzy, Structural aspects of the swelling of β chitin in hcl and its conversion into α chitin, Macromolecules 30 (1997) 3867–3873.
[34] D.A. Skoog, Principios de Análisis Instrumental, 5th ed., McGraw-Hill, Madrid, España, 2001.
[35] S. Altenor, B. Carene, E. Emmanuel, J. Lambert, J.-J. Ehrhardt, S. Gaspard, Adsorption studies of methylene blue and phenol onto vetiver roots activated carbon prepared by chemical activation, J. Hazard. Mater. 165 (2009) 1029–1039.
[36] D. Fu, Y. Zhang, F. Lv, P.K. Chu, J. Shang, Removal of organic materials from TNT red water by Bamboo Charcoal adsorption, Chem. Eng. J. 193–194 (2012) 39–49.
[37] M. Hadi, M.R. Samarghandi, G. McKay, Equilibrium two-parameter isotherms of acid dyes sorption by activated carbons: study of residual errors, Chem. Eng. J. 160 (2010) 408–416.
[38] D. Kumar, L.K. Pandey, J.P. Gaur, Evaluation of various isotherm models, and metal sorption potential of cyanobacterial mats in single and multi-metal systems, Colloids Surf., B 81 (2010) 476–485.
[39] K.Y. Foo, B.H. Hameed, Insights into the modeling of adsorption isotherm systems, Chem. Eng. J. 156 (2010) 2–10.
[40] A.Y. Dursun, O. Tepe, G. Uslu, G. Dursun, Y. Saatci, Kinetics of Remazol Black B adsorption onto carbon prepared from sugar beet pulp, Environ. Sci. Pollut. Res. 20 (2013) 2472–2483.
[41] Z. Eren, F.N. Acar, Adsorption of reactive black 5 from an aqueous solution: equilibrium and kinetic studies, Desalination 194 (2006) 1–10.
[42] F. He, J. Fan, D. Ma, L. Zhang, C. Leung, H.L. Chan, The attachment of Fe_3O_4 nanoparticles to graphene oxide by covalent bonding, Carbon 48 (2010) 3139–3144.
[43] D. Wu, P. Zheng, P.R. Chang, X. Ma, Preparation and characterization of magnetic rectorite/iron oxide nanocomposites and its application for the removal of the dyes, Chem. Eng. J. 174 (2011) 489–494.
[44] Y.S. Ho, G. McKay, The kinetics of sorption of divalent metal ions onto sphagnum moss peat, Water Res. 34 (2000) 735–742.
[45] T.S. Anirudhan, S.R. Rejeena, A.R. Tharun, Preparation, characterization and adsorption behavior of tannin-modified poly(glycidylmethacrylate)-grafted zirconium oxide-densified cellulose for the selective separation of bovine serum albumin, Colloids Surf. B 93 (2012) 49–58.
[46] S. Lagergren, About the theory of so-called adsorption of soluble substances, K. Sven. Vetenskapsakademiens Handl. 24 (1898) 1–39.
[47] A.B. Pérez-Marín, V.M. Zapata, J.F. Ortuño, M. Aguilar, J. Sáez, M. Lloréns, Removal of cadmium from aqueous solutions by adsorption onto orange waste, J. Hazard. Mater. 139 (2007) 122–131.
[48] S.W. Won, M.H. Han, Y.-S. Yun, Different binding mechanisms in biosorption of reactive dyes according to their reactivity, Water Res. 42 (2008) 4847–4855.
[49] A.-H. Chen, Y.-Y. Huang, Adsorption of Remazol Black 5 from aqueous solution by the templated crosslinked-chitosans, J. Hazard. Mater. 177 (2010) 668–675.
[50] J.-L. Gong, B. Wang, G.-M. Zeng, C.-P. Yang, C.-G. Niu, Q.-Y. Niu, et al., Removal of cationic dyes from aqueous solution using magnetic multi-wall carbon nanotube nanocomposite as adsorbent, J. Hazard. Mater. 164 (2009) 1517–1522.